Tuning Kerr-Soliton Frequency Combs to Atomic Resonances

Su-Peng Yu, Travis C. Briles, Gregory T. Moille, Xiyuan Lu, Scott A. Diddams, Kartik Srinivasan, and Scott B. Papp

Tuning Kerr-Soliton Frequency Combs to Atomic Resonances

Su-Peng Yu,[1,2,*] Travis C. Briles,[1,2] Gregory T. Moille,[3,4] Xiyuan
Lu,[3,4] Scott A. Diddams,[1,2] Kartik Srinivasan,[3] and Scott B. Papp[1,2,†]

[1]*Time and Frequency Division, NIST, Boulder, Colorado 80305, USA*
[2]*Department of Physics, University of Colorado, Boulder, Colorado 80309, USA*
[3]*Microsystems and Nanotechnology Division, NIST, Gaithersburg, Maryland 20899, USA*
[4]*Maryland Nanocenter, University of Maryland, College Park, Maryland 20740, USA*

Frequency combs based on nonlinear-optical phenomena in integrated photonics are a versatile light source that can explore new applications, including frequency metrology, optical communications, and sensing. We demonstrate robust frequency-control strategies for near-infrared, octave-bandwidth soliton frequency combs, created with nanofabricated silicon-nitride ring resonators. Group-velocity-dispersion engineering allows operation with a 1064 nm pump laser and generation of dual-dispersive-wave frequency combs linking wavelengths between approximately 767 nm and 1556 nm. To tune the mode frequencies of the comb, which are spaced by 1 THz, we design a photonic chip containing 75 ring resonators with systematically varying dimensions and we use 50 °C of thermo-optic tuning. This single-chip frequency comb source provides access to every wavelength including those critical for near-infrared atomic spectroscopy of rubidium, potassium, and cesium. To make this possible, solitons are generated consistently from device-to-device across a single chip, using rapid pump frequency sweeps that are provided by an optical modulator.

PACS numbers: 42.82.-m 42.60.Da 42.62.Eh 42.65.Tg

I. INTRODUCTION

Recently, there has been significant effort to develop chip-scale and integrated-photonics light sources and devices through nonlinear optics [1]. These have ranged from the development of ultra-stable CW lasers based on stimulated Brillouin scattering [2, 3] to metrology with frequency combs based on supercontinuum generation in photonic waveguides [4, 5] to dissipative-Kerr-soliton (DKS) formation in microresonators [6, 7]. Such soliton microcombs exhibit interesting nonlinear optical phenomena, including breathing oscillations [8–10], dark-pulse formation [11] and soliton crystallization [12], and have enabled diverse applications like communications [13], and optical-frequency synthesis [14]. DKS combs have been demonstrated with a variety of materials, including fused silica fiber and microresonators [15, 16], crystalline magnesium fluoride [17] and silicon nitride (Si_3N_4 hereafter SiN)[18–20]. SiN is an appealing material for broad bandwidth combs due to its moderately high Kerr nonlinearity and low optical propagation loss. Additionally, it is compatible with standard lithographic fabrication techniques, allowing for reliable fabrication of resonators and integration with other photonic elements [1], providing a path for broadband, low-power consumption frequency combs on a photonic chip [21].

Realizing DKS frequency combs that interface with optical-atomic transitions opens up timekeeping and other measurement applications. However alkali or alkaline-earth atomic resonances are largely prevalent in the 700 to 1000 nm spectral region, whereas many DKS experiments have operated in the 1550 nm band due to the availability of pump lasers, optical amplifiers, filters, detectors, and other components. Previous optical-clock demonstrations with soliton microcombs were pumped at 1550 nm [22, 23], and required second-harmonic generation to access atomic transitions. Moreover, atomic transitions are spectrally narrow and thus require finely tuning a frequency comb to reach resonance.

A central facet of designing DKS combs for the near-infrared [24] is that the very high microwave-to-THz repetition frequencies of microcombs and their ultrabroad-bandwidth spectra are almost exclusively determined by the geometry of the devices. A recipe has emerged to design and realize soliton microcombs at 1550 nm for some applications like optical-frequency synthesis [20]. The first step in designing the soliton spectrum is to select device geometries with anomalous group-velocity-dispersion (GVD) near the chosen pump wavelength [25]. A second step is to design higher than 2nd-order GVD contributions for generation of dispersive waves (DWs) [26], which lead to a localized increase in optical power at the edges of the soliton spectrum. A third step is tuning the carrier-envelope offset frequency of the soliton microcomb for compatibility with electronic detection on available high-speed photodetectors with bandwidth $\leq$ 20GHz.

Here, we explore frequency control and tuning of octave-spanning, near-infrared (NIR) soliton microcombs pumped at 1064 nm, towards use in atomic spectroscopy. We demonstrate a combination of GVD control of the comb's spectrum and thermo-optic frequency tuning for a single-chip solution to interface with rubidium (780 nm), cesium (852 nm), and potassium (767 nm) atoms. The advantage of a 1064 nm pump laser is that it bisects the frequency span between telecom wavelengths (1300 to 1600 nm) and atomic species that are commonly used
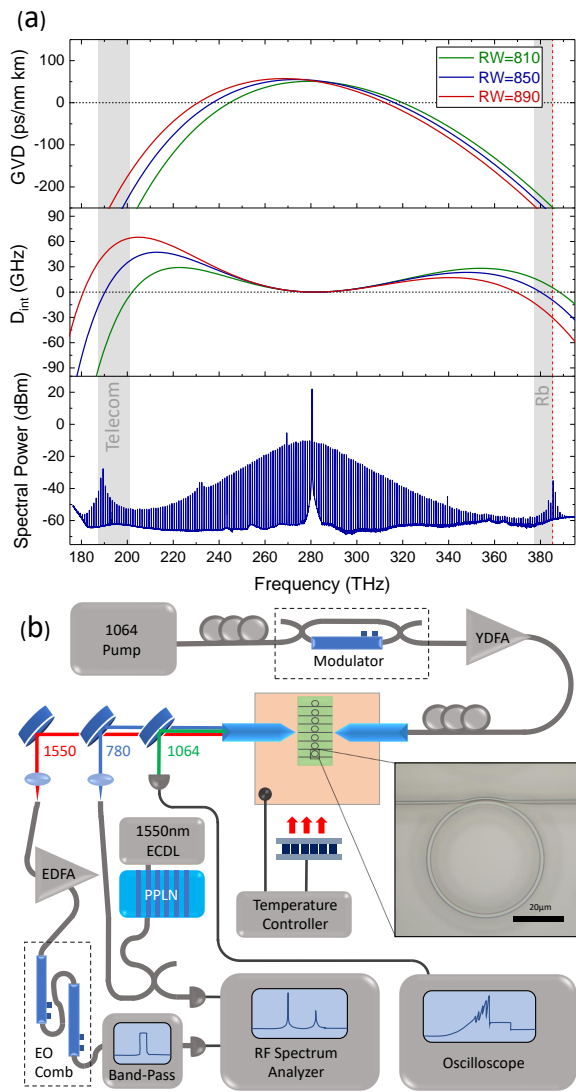
FIG. 1. Resonator dispersion design and experimental setup.
(a) The calculated GVD profile (top) and integrated modal
dispersion (middle) for ring resonators with material thickness
667nm, radius of 22.5 μm and RW of 810 nm, 850 nm, and 890
nm. The experimentally generated single soliton spectrum
from the RW=850 nm device (bottom) has its strongest SDW
line aligned to the Rb 2-hν transition (red dashed line). (b)
The experimental setup for soliton generation and comb di-
agnostics. An ECDL is coupled to a Mach-Zehnder intensity-
modulator, amplified in a YDFA and coupled into the pho-
tonic chip using lensed fibers and precision positioning stages.
The generated comb light is separated into spectral bands
centered at 780, 1064 and 1550 nm for subsequent diagnos-
tics. Each branch can be monitored in real time or undergo
heterodyne with local oscillators. The notch filter used in the
1064 nm branch to reject pump light when monitoring soliton
generation, is not shown. The long-wavelength DW branch
is amplified using EDFA to provide optical power for further
measurement steps.

for atomic clocks like strontium (699 nm) and calcium ion
(729 nm) [27–29]. Our soliton microcomb provides up to

0.3 μW per mode over the 760 to 900 nm range of interest
for atomic spectroscopy, and also few μW per mode in
the Telecom bands. The comb is pumped with standard
1064 nm laser technology, and we demonstrate high co-
herence with the soliton microcomb through detection of
its 1 THz repetition frequency and f-$2f$ measurements.

II. SOLITON MICROCOMB DESIGN

The photonic-chip resonators in this study are SiN
microring resonators embedded in a silicon-dioxide
cladding. A ring radius of 22.5 μm (center of wavg-
uide) is chosen to give a free-spectral range (FSR) of ≈ 1
THz, which reduces the comb operating power [20]. The
devices are fabricated at wafer scale by Ligentec, using
LPCVD stoichiometric silicon-nitride deposition, DUV
stepper lithography, dry chemical etching, and separation
to individual chips. Broadband, weakly anomalous GVD
is created near the 1064 nm pump laser wavelength by
design of the resonator dimensions, namely the SiN layer
thickness and resonator waveguide width (RW). GVD
simulations for resonators with a SiN layer thickness of
667 nm and RW = 810, 850 and 890 nm illustrate the soli-
ton microcomb design process; see the top panel of Fig.
1(a). We indicate the telecom bands (1500-1600 nm) and
the NIR range relevant for rubidium atomic spectroscopy
(778-795 nm) with vertical gray boxes.

Our resonators also support the generation of DWs
that extend the soliton spectrum outside the anomalous-
GVD region. The emitted DWs correspond approxi-
mately to the wavelengths of zero integrated dispersion,
D_{int} [18]. The integrated dispersion is equivalent to
the detuning of the cold-resonator frequencies ν_μ from
an equidistant grid centered about the pump laser and
spaced by the free spectral range (FSR) about the pump
laser,

$$D_{int}(\mu) = \nu_\mu - \left(\nu_p - \mu \times \frac{D_1}{2\pi} \right) \quad (1)$$

Here, ν_p is the pump laser frequency, $\frac{D_1}{2\pi}$ is the resonator
FSR near the pump and μ is an integer indexing the res-
onances relative to the pumped mode $\mu = 0$. This quan-
tity, given in units of GHz, is plotted in the middle panel
of Fig. 1(a) for the three corresponding traces in the top
panel. We note that increasing the resonator waveguide-
width (RW) parameter leads to an overall redshift of the
GVD profile as well as the wavelengths of $D_{int} = 0$. Since
both the device layer thickness and RW affect the GVD
profile, we can quasi-independently design and control
the peak wavelength of the two DWs.

The linear approximation for the DW wavelengths
given by $D_{int}(\mu) = 0$ neglects higher-order effects aris-
ing from soliton self-phase modulation [30]. However, it
is a reasonable criteria for predicting the performance
of resonator designs given the fabrication tolerances of
~ 5 nm in device layer thickness and ~ 20 nm in pat-
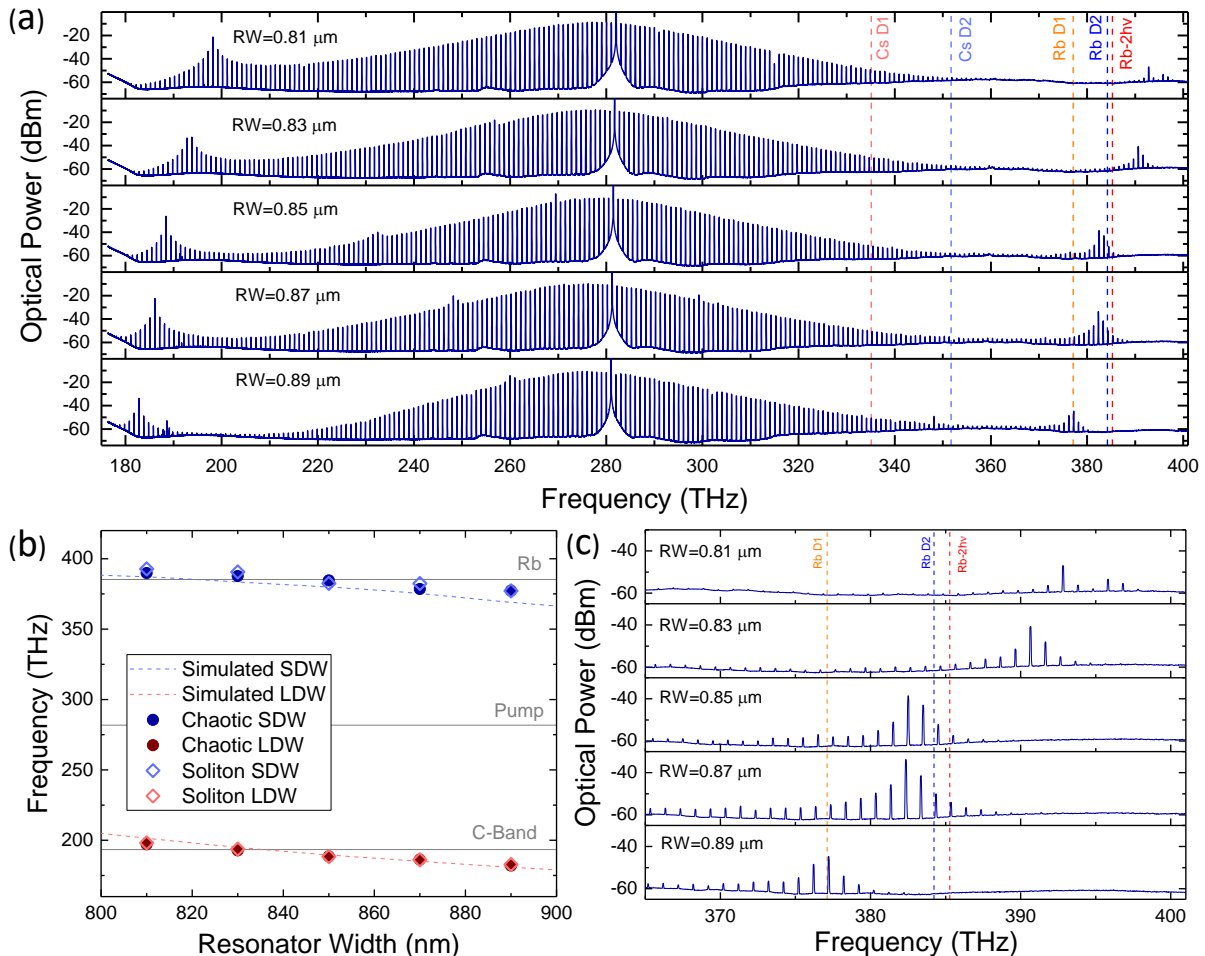tern dimensions, including effects of waveguide sidewall

FIG. 2. Soliton microcomb spectrum control through nanofabrication. (a) Single-soliton spectra obtained from resonators with varying waveguide widths on the same chip. Relevant atomic transitions are indicated on the plot. The on-chip, single-sideband pump powers are from top to bottom 160 mW, 180 mW, 175 mW, 190 mW and 160 mW. (b) Comparison between measured dispersive wave frequencies and that predicted by simulated waveguide dispersion show good agreement within fabrication imprecision of resonator dimensions. (c) A zoom in plot near the rubidium optical transition frequencies.

angle. These small deviations are accounted for by fabricating resonators of various RW values, stepped by 10's of nanometers, on a single chip. We design chips composed of ∼75 individual ring resonators to systematically cover the microcomb design space.

The bottom panel of Fig. 1(a) shows the result of controllably taking advantage of the microcomb design space in SiN. The soliton microcomb spectrum that we present features a long-wavelength DW in the telecom band and short-wavelength DW with its strongest line aligned to the Rb 2-photon clock transition at 778 nm [31–33].

III.   OPTICAL MEASUREMENT

The setup we use for our experiments is shown in Fig. 1(b). In particular, the apparatus is composed of elements for soliton microcomb generation and thermo-optic tuning, and for coherence measurements of the soliton microcomb's carrier-envelope-offset frequency and repetition frequency. The pump laser we use is an external cavity diode laser, providing coarse tuning from 1020 to 1070 nm to address a few of the TE1 ring resonator modes that are spaced by 1 THz.

In order to provide laser light to our resonators, coupling waveguides are fabricated in the silicon nitride device layer. Inverse tapering of the coupling waveguide at chip edge enables approximately 3 dB per facet insertion loss from standard lensed fibers. A 'pulley' design [20, 34, 35] for the coupling waveguide achieves adequate coupling rates for low-power operation of the comb and also at the edges of the spectrum for output-coupling of the dispersive waves. We include a variation in the coupling gap between the pulley coupler and the resonator to achieve critical coupling, namely, to set the coupling strength between the resonator and the coupling waveguide to match the internal loss of the resonator. This cou-

pling condition maximizes the intra-resonator power for a given pump power, reducing the pump power required to support soliton microcombs. We extract information on the intrinsic and coupled quality factor by measuring the resonance linewidth and minimum transmission as a function of gap. The spectra shown in Figs 1(a) and 2 were obtained using resonators with intrinsic quality factors of $\approx 1 \times 10^6$ and comb generation threshold powers as low as 9 mW in the coupling waveguide. Ongoing experiments show that intrinsic Q's up to $\approx 3 \times 10^6$ and threshold powers of 1 mW are possible at 1064 nm.

We efficiently generate soliton microcombs by controlling the pump-resonator detuning at a rate faster than the resonator thermal dynamics [36–38]. This is implemented using an ultrafast electro-optic frequency shifting technique similar to that reported in Ref [20]. Here we utilize a standard lithium-niobate waveguide Mach-Zehnder intensity modulator in place of the single-sideband, suppressed-carrier modulator. The output of the intensity modulator is passed to a polarization controller and amplified in an ytterbium-doped fiber amplifier (YDFA) before being coupled into the chip. The blue-detuned sideband frequency is tuned to resonance and then decreased by ≈ 5 GHz in 100 ns. This rapid pump frequency tuning technique minimizes the thermo-optic shift of the resonance frequency, which can destabilize the soliton. The red sideband and residual carrier are far detuned (by ≥ 20 resonator linewidths) from any resonances and do not adversely affect soliton generation. We filter out the pump light to monitor the generated comb power. The emergence of soliton microcombs from chaotic states as we vary the detuning is identified from the photodetected comb power, using an oscilloscope; see the trace plotted in Fig. 1(b).

Optical spectra of single-soliton microcombs that we create are shown in Fig. 2(a). We present spectra for five RW values, spaced by 20 nm from RW = 810-890 nm. The spectra were obtained with on-chip, single-sideband pump powers between 160-190 mW. Note that the comb line corresponding to the pump laser is graphically suppressed for compact display of the data. Each spectrum features two prominent dispersive waves on either side of the pump laser. The long-wavelength DW's (LDW) are in the telecom C/L band and the short-wavelength DW's (SDW) are in the NIR 780 nm band. The LDW and SDW are plotted versus RW in Fig. 2(b) as hollow red and blue diamonds, respectively. For comparison, we also present DW frequency measurements obtained with blue-detuned chaotic combs (solid circles). This thorough and unique comparison of microcomb spectra is enabled by precision fabrication of numerous devices and reliable soltion microcomb generation. Our measurements of the DW frequencies agree with our designs, which are based on finite-element calculations of D_{int} (open circles), using accurate Sellmeier coefficients for SiN [39] and silica [40] and a fabrication precision that we assess to be ~ 20 nm. The predictability of dispersive wave frequencies enables placement of dispersive waves on the

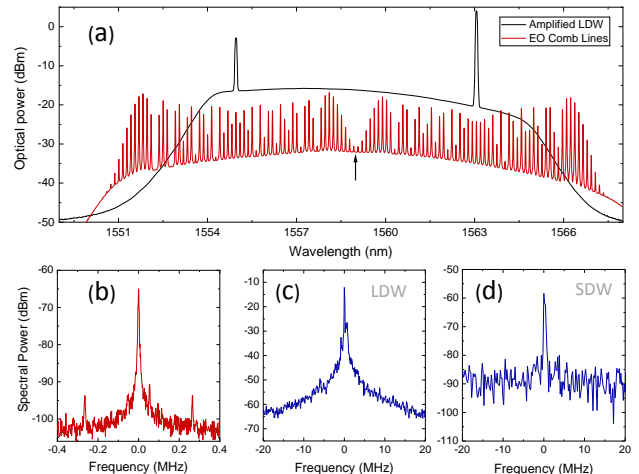targeted Rb resonances, as shown in the zoom-in plot in Fig. 3(c).

FIG. 3. Soliton coherence measurements. (a) The filtered and amplified long-wavelength DW before (black) and after (red) being sent to electro-optic phase modulators. A heterodyne beat is made at the wavelength marked with an arrow to evaluate fluctuations in THz comb mode spacing. This beat is shown in (b). (c,d) Heterodyne beats of each DW with a low-noise auxiliary laser: (c) LDW at 1563 nm and (d) SDW at 777.3 nm. The traces (b) through (d) are taken with resolution bandwidth 1 kHz, 100 kHz, and 300 kHz, respectively.

We measure the repetition frequency of the soliton microcomb by electro-optic modulation of the LDW near 1550 nm. Such measurements are shown for the RW=0.83 μm device in Fig. 3. This procedure creates a low frequency <100 MHz optical heterodyne beatnote f_{beat} that represents the 0.999291 THz repetition frequency. To facilitate these measurements, we use optical filters to isolate the dispersive waves near 1550 nm and 780 nm. The long-wavelength DW is amplified with a C-band erbium-doped fiber amplifier (EDFA), filtered, and sent to two electro-optic phase modulators operating in series and driven at $f_{eo} \approx 16.65$ GHz to create many coherent sidebands around each comb tooth [41]. We detect f_{beat} by photodetecting the phase modulation sidebands nearly in between the two soliton microcomb modes, allowing the repetition frequency to be determined via $f_{rep} = 60 \cdot f_{eo} + f_{beat}$. A narrow optical bandpass filter selects the desired interfering modes (marked with an arrow in Fig. 3(a)) before photodetecting f_{beat}. The highly coherent beat obtained from this measurement (shown in Fig. 3(b)) confirms low-noise soliton operation.

We evaluate the frequency noise on individual comb modes by recording optical heterodyne beats between the soliton comb and an auxiliary low-noise CW laser. We focus on large comb mode numbers at a large frequency offset from the 1064 nm pump laser, which are interesting to test since they are most sensitive to multiplicative noise of the comb. A C-band external cavity diode

laser is heterodyned directly with the long-wavelength DW near 1563 nm, and it is also frequency doubled in a bulk periodically poled lithium niobate crystal for the short-wavelength DW near 777.3 nm. For both heterodyne beatnotes, which are shown in Figs. 3 (c) and (d) for the long- and short-wavelength DW, respectively, we observe linewidths of a few megahertz that we associate with the linewidth of the soliton microcomb modes. This is reasonable considering that the free-running repetition rate has a frequency linewidth of ≈5 kHz and the comb modes we characterize in Figs. 3 (c) and (d) are ≈100 modes from the pump.

We note that the DW wavelengths were chosen in this case to be near-harmonic to facilitate f-$2f$ referencing. For this particular device, the offset frequency f_0 is ≈ 80 ± 1 GHz. While such a high frequency makes a direct electronic measurement of f_0 challenging, in future designs we would systematically vary the resonator radius in steps of ≈ 10 nm to create a specific device that satisfies the condition $f_0 \leq 20$ GHz [20].

IV. THERMO-OPTIC FINE TUNING

We finely shift the absolute frequencies of the soliton comb modes beyond the level provided by nanofabrication process control, using thermo-optic tuning of the resonator. This approach combines the high optical power per mode of DKS combs with the high spectral resolution typical of lower repetition rate combs [42]. The temperature of the chip is set with a PID-controlled thermoelectric heater; see Fig. 1 (b) for the setup. Fig 4 (a) and (b) analyze the thermal tuning of solitons created in RW = 0.87 μm resonators (second to last panel in Fig. 2 (a) and (c)). Comb modes near 778 nm have a measured tuning coefficient of -5.48 GHz/ °C which is sufficiently large to access the Rb $2h\nu$ and D2 resonances at chip temperatures of ≈ 37 and ≈ 44 °C respectively; see Fig. 4(a). The change in the comb modes power between these two temperatures is associated with hysteresis in switching behavior between distinct operating regimes of the single soliton pulse. This behavior is attributed to interference between phase dependent, extended CW background and DW intensities similar to recent theoretical [30] and experimental work [43] and will be explored in more detail in future work. The measured linear thermal tuning of the soliton repetition rate of 15.86±0.34 MHz /°C shown in Fig. 4 (b) amounts to a fractional change of ≈ 16 ppm on the 1.0 THz spacing. This is in reasonable agreement with measured thermo-optic coefficients of bulk silicon nitride at 20 to 30 ppm [44]as well as experimental measurements on resonators pumped at 1550 nm [45], with potentially a weak component from thermal expansion of the ring geometry with the same sign [46]. Temperature variations in the offset frequency can be approximated by $\frac{df_0}{dT} = \left(\frac{dn_g}{dT} - \frac{dn_p}{dT}\right)\frac{f_p}{n_g}$ where n_p and n_g are the phase and group indexes of refraction and f_p is the pump frequency [45]. Because $\frac{dn_g}{dT}$ and $\frac{dn_p}{dT}$ are of similar magnitude tem-

perature variations have a comparatively small effect of f_0. In future work we plan to incorporate integrated heaters [45, 47], which will reduce the overall electrical power consumption.
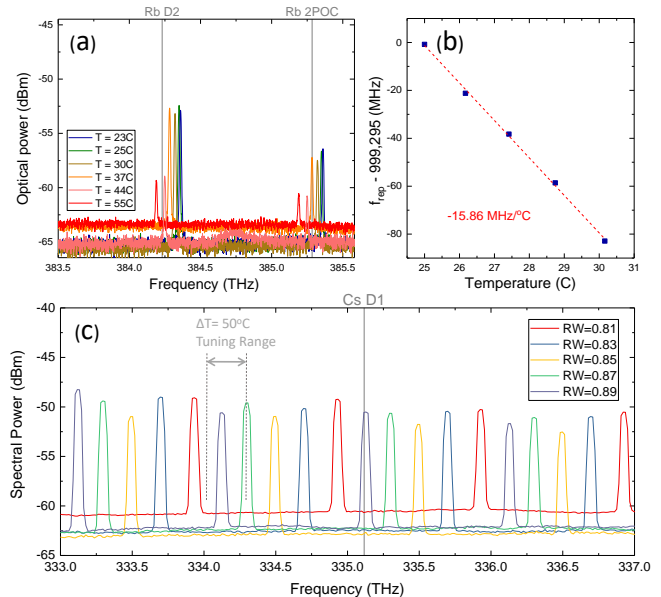

FIG. 4. Thermo-optic tuning of soliton spectrum. (a) The thermal tuning of two modes of the soliton spectrum across the Rb two-photon and Rb D2 transitions. (b) The repetition rate of the soliton can also be thermally tuned. (c) Overlay of the spectra presented in Fig. 2 plotted over the range from 333 to 337 THz. Note that any arbitrary frequency can be reached with the current RW sweep and a 50 °C thermal tuning range.

Through both lithographic variation in resonator dimensions and thermo-optic tuning, we exert comprehensive frequency control over the SiN comb. A typical chip used in this study contains 70 devices, which is sufficient to include combinations of fine resonator width and gap sweeps for desired dispersion and coupling. A modest $\Delta T = 50$ °C thermal-optic tuning of the chip is sufficient to place a comb line onto any desired wavelength within the design bandwidth of the resonators. For example, to probe the cesium D1 transition, we can select a device with RW=870 nm or 890 nm, and thermally tune the modes toward lower frequency to align to the desired transition, as shown in Fig. 4(c).

V. CONCLUSION

We have presented Kerr-soliton frequency combs operating in the near infrared using silicon nitride microresonators. Dispersion engineering of the resonator waveguide provides octave bandwidth through the emission of dual dispersive waves at predictable wavelengths on either side of the pump laser. Further, our chosen design wavelengths for the pump laser as well as both the long- and short-wavelength DW's offer significant advantages

for future compact comb systems. Pumping at 1064 nm allows for robust generation of low noise solitons using fast frequency sweeps from standard electro-optic intensity modulators. Full stabilization of the comb could be straightforwardly accomplished by leveraging the LDW's position in the telecom C/L band using mature optical technology such as erbium amplifiers, efficient second harmonic generators and optical modulators. The SDW is ideal for applications requiring high power per mode in the 760-900 nm NIR band. We have demonstrated the flexibility of our system by thermally tuning optical comb modes to continuously fill in wide bandwidths across the near infrared, and onto Rb and Cs resonances. This tunability will enable future experiments exploring spectroscopy and metrology with atomic resonances.

[1] David J Moss, Roberto Morandotti, Alexander L Gaeta, and Michal Lipson, "New cmos-compatible platforms based on silicon nitride and hydex for nonlinear optics," Nature Photonics **7**, 597–607 (2013).

[2] Jiang Li, Hansuek Lee, and Kerry J Vahala, "Microwave synthesizer using an on-chip brillouin oscillator," Nature Communications **4**, 2097 (2013).

[3] William Loh, Adam AS Green, Fred N Baynes, Daniel C Cole, Franklyn J Quinlan, Hansuek Lee, Kerry J Vahala, Scott B Papp, and Scott A Diddams, "Dual-microcavity narrow-linewidth brillouin laser," Optica **2**, 225–232 (2015).

[4] David R Carlson, Daniel D Hickstein, Alex Lind, Stefan Droste, Daron Westly, Nima Nader, Ian Coddington, Nathan R Newbury, Kartik Srinivasan, Scott A Diddams, and Scott B Papp, "Self-referenced frequency combs using high-efficiency silicon-nitride waveguides," Optics letters **42**, 2314–2317 (2017).

[5] Erin S Lamb, David R Carlson, Daniel D Hickstein, Jordan R Stone, Scott A Diddams, and Scott B Papp, "Optical-frequency measurements with a kerr microcomb and photonic-chip supercontinuum," Physical Review Applied **9**, 024030 (2018).

[6] T Herr, V Brasch, JD Jost, CY Wang, NM Kondratiev, ML Gorodetsky, and TJ Kippenberg, "Temporal solitons in optical microresonators," Nature Photonics **8**, 145–152 (2014).

[7] Tobias J Kippenberg, Alexander L Gaeta, Michal Lipson, and Michael L Gorodetsky, "Dissipative kerr solitons in optical microresonators," Science **361**, eaan8083 (2018).

[8] Chengying Bao, Jose A Jaramillo-Villegas, Yi Xuan, Daniel E Leaird, Minghao Qi, and Andrew M Weiner, "Observation of fermi-pasta-ulam recurrence induced by breather solitons in an optical microresonator," Physical Review Letters **117**, 163901 (2016).

[9] Erwan Lucas, Maxim Karpov, H. Guo, ML Gorodetsky, and Tobias J. Kippenberg, "Breathing dissipative solitons in optical microresonators," Nature Communications **8**, 736 (2017).

[10] Mengjie Yu, Jae K Jang, Yoshitomo Okawachi, Austin G Griffith, Kevin Luke, Steven A Miller, Xingchen Ji, Michal Lipson, and Alexander L Gaeta, "Breather soliton dynamics in microresonators," Nature Communications **8**, 14569 (2017).

[11] Xiaoxiao Xue, Yi Xuan, Yang Liu, Pei-Hsun Wang, Steven Chen, Jian Wang, Dan E Leaird, Minghao Qi, and Andrew M Weiner, "Mode-locked dark pulse kerr combs in normal-dispersion microresonators," Nature Photonics **9**, 594 (2015).

[12] Daniel C Cole, Erin S Lamb, Pascal Del'Haye, Scott A Diddams, and Scott B Papp, "Soliton crystals in kerr resonators," Nature Photonics **11**, 671 (2017).

[13] Pablo Marin-Palomo, Juned N Kemal, Maxim Karpov, Arne Kordts, Joerg Pfeifle, Martin HP Pfeiffer, Philipp Trocha, Stefan Wolf, Victor Brasch, Miles H Anderson, Ralf Rosenberger, Kovendham Vijayan, Wolfgang Freude, Tobias J Kippenberg, and Christian Koos, "Microresonator-based solitons for massively parallel coherent optical communications," Nature **546**, 274 (2017).

[14] Daryl T Spencer, Tara Drake, Travis C Briles, Jordan Stone, Laura C Sinclair, Connor Fredrick, Qing Li, Daron Westly, B Robert Ilic, Aaron Bluestone, Nicolas Volet, Tin Komljenovic, Lin Chang, Seung Hoon Lee, Dong Yoon Oh, Myoung-Gyun Suh, Ki Youl Yang, Martin H. P. Pfeiffer, Tobias J. Kippenberg, Erik Norberg, Luke Theogarajan, Kerry Vahala, Nathan R. Newbury, Kartik Srinivasan, John E. Bowers, Scott A. Diddams, and Scott B. Papp, "An optical-frequency synthesizer using integrated photonics," Nature **557**, 81–85 (2018).

[15] Xu Yi, Qi-Fan Yang, Ki Youl Yang, Myoung-Gyun Suh, and Kerry Vahala, "Soliton frequency comb at microwave

[16] Yadong Wang, François Leo, Julien Fatome, Miro Erkintalo, Stuart G Murdoch, and Stéphane Coen, "Universal mechanism for the binding of temporal cavity solitons," Optica **4**, 855–863 (2017).

[17] Andrey B Matsko, Wei Liang, Anatoliy A Savchenkov, Danny Eliyahu, and Lute Maleki, "Optical cherenkov radiation in overmoded microresonators," Optics letters **41**, 2907–2910 (2016).

[18] Victor Brasch, Michael Geiselmann, Tobias Herr, Grigoriy Lihachev, Martin HP Pfeiffer, Michael L Gorodetsky, and Tobias J Kippenberg, "Photonic chip–based optical frequency comb using soliton cherenkov radiation," Science **351**, 357–360 (2016).

[19] Jose A Jaramillo-Villegas, Xiaoxiao Xue, Pei-Hsun Wang, Daniel E Leaird, and Andrew M Weiner, "Deterministic single soliton generation and compression in microring resonators avoiding the chaotic region," Optics Express **23**, 9618–9626 (2015).

[20] Travis C Briles, Jordan R Stone, Tara E Drake, Daryl T Spencer, Connor Fredrick, Qing Li, Daron Westly, BR Ilic, Kartik Srinivasan, Scott A Diddams, and Scott B. Papp, "Interlocking kerr-microresonator frequency combs for microwave to optical synthesis," Optics Letters **43**, 2933–2936 (2018).

[21] Brian Stern, Xingchen Ji, Yoshitomo Okawachi, Alexander L Gaeta, and Michal Lipson, "Battery-operated integrated frequency comb generator," Nature , 1 (2018).

[22] Scott B Papp, Katja Beha, Pascal Del'Haye, Franklyn Quinlan, Hansuek Lee, Kerry J Vahala, and Scott A Diddams, "Microresonator frequency comb optical clock," Optica **1**, 10–14 (2014).

[23] Z L Newman, V Maurice, T E Drake, J R Stone, T C Briles, D T Spencer, C Fredrick, Q Li, D Westly, B R Ilic, B Shen, K Y Yang, C Johnson, M S Johnson, L Hollberg, K Vahala, K Srinivasan, S A Diddams, J Kitching, S B Papp, and M T Hummon, "Photonic integration of an optical atomic clock," arXiv preprint arXiv:1811.00616 (2018).

[24] Maxim Karpov, Martin H. P. Pfeiffer, Junqiu Liu, Anton Lukashchuk, and Tobias J. Kippenberg, "Photonic chip-based soliton frequency combs covering the biological imaging window," Nature Communications **9** (2018), 10.1038/s41467-018-03471-x.

[25] Imad H Agha, Yoshitomo Okawachi, and Alexander L Gaeta, "Theoretical and experimental investigation of broadband cascaded four-wave mixing in high-q microspheres," Optics Express **17**, 16209–16215 (2009).

[26] Yoshitomo Okawachi, Michael RE Lamont, Kevin Luke, Daniel O Carvalho, Mengjie Yu, Michal Lipson, and Alexander L Gaeta, "Bandwidth shaping of microresonator-based frequency combs via dispersion engineering," Optics Letters **39**, 3535–3538 (2014).

[27] Scott A Diddams, James C Bergquist, Steven R Jefferts, and Christopher W Oates, "Standards of time and frequency at the outset of the 21st century," Science **306**, 1318–1324 (2004).

[28] Andrew D Ludlow, Martin M Boyd, Jun Ye, Ekkehard Peik, and Piet O Schmidt, "Optical atomic clocks," Reviews of Modern Physics **87**, 637 (2015).

[29] R. Le Targat, L. Lorini, Y. Le Coq, M. Zawada, J. Guna, M. Abgrall, M. Gurov, P. Rosenbusch, D. G. Rovera, B. Nagrny, R. Gartman, P. G. Westergaard, M. E. Tobar, M. Lours, G. Santarelli, A. Clairon, S. Bize, P. Laurent, P. Lemonde, and J. Lodewyck, "Experimental realization of an optical second with strontium lattice clocks," Nature Communications **4** (2013), 10.1038/ncomms3109.

[30] DV Skryabin and YV Kartashov, "Self-locking of the frequency comb repetition rate in microring resonators with higher order dispersions," Optics Express **25**, 27442–27451 (2017).

[31] L Hilico, R Felder, D Touahri, O Acef, A Clairon, and F Biraben, "Metrological features of the rubidium two-photon standards of the bnm-lptf and kastler brossel laboratories," The European Physical Journal-Applied Physics **4**, 219–225 (1998).

[32] Nathan D Zameroski, Gordon D Hager, Christopher J Erickson, and John H Burke, "Pressure broadening and frequency shift of the $5s_{1/2} \to 5d_{5/2}$ and $5s_{1/2} \to 7s_{1/2}$ two photon transitions in 85 rb by the noble gases and n_2," Journal of Physics B: Atomic, Molecular and Optical Physics **47**, 225205 (2014).

[33] JE Bernard, AA Madej, KJ Siemsen, L Marmet, C Latrasse, D Touahri, M Poulin, M Allard, and M Têtu, "Absolute frequency measurement of a laser at 1556 nm locked to the $5s_{1/2}$- $5d_{5/2}$ two-photon transition in 87rb," Optics Communications **173**, 357–364 (2000).

[34] Ehsan Shah Hosseini, Siva Yegnanarayanan, Amir Hossein Atabaki, Mohammad Soltani, and Ali Adibi, "Systematic design and fabrication of high-q single-mode pulley-coupled planar silicon nitride microdisk resonators at visible wavelengths," Optics Express **18**, 2127–2136 (2010).

[35] Qing Li, Travis C Briles, Daron Westly, Jordan Stone, Robert Ilic, Scott Diddams, Scott Papp, and Kartik Srinivasan, "Octave-spanning microcavity kerr frequency combs with harmonic dispersive-wave emission on a silicon chip," in *Frontiers in Optics* (Optical Society of America, 2015) pp. FW6C–5.

[36] Travis C. Briles, Jordan R. Stone, Tara E Drake, Daryl T. Spencer, Scott A. Diddams, and Scott B. Papp, "Manuscript in preparation," In preparation (2018).

[37] Jordan R Stone, Travis C Briles, Tara E Drake, Daryl T Spencer, David R Carlson, Scott A Diddams, and Scott B Papp, "Thermal and nonlinear dissipative-soliton dynamics in kerr-microresonator frequency combs," Physical Review Letters **121**, 063902 (2018).

[38] Qing Li, Travis C Briles, Daron A Westly, Tara E Drake, Jordan R Stone, B Robert Ilic, Scott A Diddams, Scott B Papp, and Kartik Srinivasan, "Stably accessing octave-spanning microresonator frequency combs in the soliton regime," Optica **4**, 193–203 (2017).

[39] Kevin Luke, Yoshitomo Okawachi, Michael R. E. Lamont, Alexander L. Gaeta, and Michal Lipson, "Broadband mid-infrared frequency comb generation in a si3n4 microresonator," Optics Letters **40** (2015), 10.1364/OL.40.004823.

[40] I. H. Malitson, "Interspecimen comparison of the refractive index of fused silica," Journal of the Optical Society of America **55**, 1205–1209 (1965).

[41] Pascal Del'Haye, Scott B Papp, and Scott A Diddams, "Hybrid electro-optically modulated microcombs," Physical Review Letters **109**, 263901 (2012).

[42] D. C. Heinecke, A. Bartels, T. M. Fortier, D. A. Braje, L. Hollberg, and S. A. Diddams, "Optical frequency stabilization of a 10 ghz ti:sapphire frequency comb by satu-

rated absorption spectroscopy in rubidium 87," Physical Review A **80**, 053806 (2009).

[43] Travis C Briles, Jordan R Drake, Daryl T Spencer, Connor Frederick, Qing Li, Daron A Westly, B Robert Illic, Kartik Srinivasan, Scott A Diddams, and Scott B Papp, "Kerr-microresonator solitons for accurate carrier-envelope-frequency stabilization," arXiv preprint arXiv:1711.06251 (2017).

[44] Kazuhiro Ikeda, Robert E Saperstein, Nikola Alic, and Yeshaiahu Fainman, "Thermal and kerr nonlinear properties of plasma-deposited silicon nitride/silicon dioxide waveguides," Optics Express **16**, 12987–12994 (2008).

[45] Xiaoxiao Xue, Yi Xuan, Cong Wang, Pei-Hsun Wang, Yang Liu, Ben Niu, Daniel E Leaird, Minghao Qi, and Andrew M Weiner, "Thermal tuning of kerr frequency combs in silicon nitride microring resonators," Optics Express **24**, 687–698 (2016).

[46] Amit Kaushik, Harold Kahn, and Arthur H. Heuer, "Wafer-level mechanical characterization of silicon nitride mems," Journal of Microelectromechanical Systems **14** (2005), 10.1109/JMEMS.2004.839315.

[47] Chaitanya Joshi, Jae K Jang, Kevin Luke, Xingchen Ji, Steven A Miller, Alexander Klenner, Yoshitomo Okawachi, Michal Lipson, and Alexander L Gaeta, "Thermally controlled comb generation and soliton mode-locking in microresonators," Optics Letters **41**, 2565–2568 (2016).